Transdermal microarrayed electroporation for enhanced cancer immunotherapy based on DNA vaccination

Wang, Yuan; Qu, Jin; Xiong, Chuxiao; Chen, Bing; Xie, Kai; Wang, Mingxue; Liu, Zhen; Yue, Zhao; Liang, Zhenghua; Wang, Feng; Zhang, Tianlong; Zhu, Guangyu; Kuang, Yi Becki; Shi, Peng

Published in:
PNAS: Proceedings of the National Academy of Sciences of the United States of America

Published: 18/06/2024

Document Version:
Final Published version, also known as Publisher's PDF, Publisher's Final version or Version of Record

Published version (DOI):
10.1073/pnas.2322264121

Publication details:
Wang, Y., Qu, J., Xiong, C., Chen, B., Xie, K., Wang, M., Liu, Z., Yue, Z., Liang, Z., Wang, F., Zhang, T., Zhu, G., Kuang, Y. B., & Shi, P. (2024). Transdermal microarrayed electroporation for enhanced cancer immunotherapy based on DNA vaccination. *PNAS: Proceedings of the National Academy of Sciences of the United States of America*, *121*(25), Article e2322264121. https://doi.org/10.1073/pnas.2322264121

PNAS RESEARCH ARTICLE | ENGINEERING CELL BIOLOGY

Transdermal microarrayed electroporation for enhanced cancer immunotherapy based on DNA vaccination

Yuan Wang[a,1], Jin Qu[a,1], Chuxiao Xiong[a], Bing Chen[b], Kai Xie[a], Mingxue Wang[a], Zhen Liu[a], Zhao Yue[c], Zhenghua Liang[d], Feng Wang[b], Tianlong Zhang[e], Guangyu Zhu[c], Yi Becki Kuang[d], and Peng Shi[a,f,g,h,2]

Affiliations are included on p. 12.

Edited by Catherine Murphy, University of Illinois at Urbana-Champaign, Urbana, IL; received December 18, 2023; accepted May 14, 2024

Despite the tremendous clinical potential of nucleic acid–based vaccines, their efficacy to induce therapeutic immune response has been limited by the lack of efficient local gene delivery techniques in the human body. In this study, we develop a hydrogel-based organic electronic device (μEPO) for both transdermal delivery of nucleic acids and in vivo microarrayed cell electroporation, which is specifically oriented toward one-step transfection of DNAs in subcutaneous antigen-presenting cells (APCs) for cancer immunotherapy. The μEPO device contains an array of microneedle-shaped electrodes with pre-encapsulated dry DNAs. Upon a pressurized contact with skin tissue, the electrodes are rehydrated, electrically triggered to release DNAs, and then electroporate nearby cells, which can achieve in vivo transfection of more than 50% of the cells in the epidermal and upper dermal layer. As a proof-of-concept, the μEPO technique is employed to facilitate transdermal delivery of neoantigen genes to activate antigen-specific immune response for enhanced cancer immunotherapy based on a DNA vaccination strategy. In an ovalbumin (OVA) cancer vaccine model, we show that high-efficiency transdermal transfection of APCs with OVA-DNAs induces robust cellular and humoral immune responses, including antigen presentation and generation of IFN-γ^{+} cytotoxic T lymphocytes with a more than 10-fold dose sparing over existing intramuscular injection (IM) approach, and effectively inhibits tumor growth in rodent animals.

transdermal gene delivery | hydrogel electronics | in vivo electroporation | cancer immunotherapy | DNA vaccination

Significance

Nucleic acid (NA)–based medicine undergoes extensive investigation as therapeutics and vaccines. Its considerable advantages have been well demonstrated in the COVID-19 pandemic, where RNAvaccines were quickly designed, scale-manufactured, and mass-distributed. However, despite the tremendous clinical potential, the success of NA-medicine for treating different human diseases has been limited has been limited, partially due to the lack of efficient in vivo gene delivery techniques, especially when the associated cytosolic delivery is required in a footprint-free manner without leaving behind any additional reagents (e.g., lipid particles) in human body. This study reports a hydrogel electronic device capable of transdermal delivery of NAs (nucleic acids) and in vivo microarrayed cell electroporation, offering a promising solution for one-step and painless transdermal gene delivery in the clinical practice of immunotherapy.

The concept of deploying the immune system as a tool to treat cancer has been explored for a long time and becomes increasingly popular in the past decade since the approval of chimeric antigen receptor (CAR) T cells for treating advanced blood cancers (1). In most cases, different cancer immunotherapies are developed with an emphasis on direct or indirect T cell engineering around three technical routes, including immune checkpoint blockade, adoptive cell infusion, or cancer vaccination (2, 3). Particularly, DNA vaccination has emerged as a promising approach that induces robust tumor-specific immune responses (4). An essential process for DNA vaccination is the intracellular delivery of nucleic acid (NA)–based vaccine materials to host cells, which are engineered to express neoantigen proteins to stimulate the immune system (5). However, the efficacy of DNA vaccination for cancer immunotherapy is largely unsatisfactory, partially due to the difficulties in antigen transportation to APCs (e.g., Langerhans cells) and a low efficiency to recruit and activate them (6). In this regard, it is important to develop techniques to improve the cytosolic delivery of tumor-specific NAs (e.g., DNA or RNA) to APCs, especially for in vivo usage in the context of cancer immunotherapy (7).

Currently, intramuscular injection (IM) is the most widely used method for delivering NAs in the animal or human body. Four out of the five DNA vaccines licensed for veterinary applications are administered through intramuscular injection of naked plasmid DNAs (8). Some human clinical trials also use the IM method (9). But the injection of naked DNAs typically yields extremely low cell transfection efficiency, which is far below the requirements for immunoactivation (10). To tackle this problem, different approaches, such as cationic lipids/polymer encapsulation, electroporation, nanoparticle-assisted system, and pressurized injection of microdroplet, have been developed and showed mixed results in enhancing DNA delivery efficiency to immune cells (10–12). The quick and wide application of RNA vaccine in the pandemic of COVID-19 has been a great success in transdermal delivery of RNAs by using a lipid nanoparticle (LNP) system (13), but the effectiveness remains to be tested for DNAs or for usage with targeting tissues in different organs. LNP material may also cause unexpected allergy in some patients (14).

Competing interest statement: P.S., J.Q., Y.W., and K.X. are listed as inventors on a patent application (US Priority No. 17/804,118) filed by the City University of Hong Kong describing the micro-electroporation-based delivery system.

This article is a PNAS Direct Submission.

[1]Y.W. and J.Q. contributed equally to this work.

[2]To whom correspondence may be addressed. Email: pengshi@cityu.edu.hk.

This article contains supporting information online at https://www.pnas.org/lookup/suppl/doi:10.1073/pnas.2322264121/-/DCSupplemental.

Published June 12, 2024.

As a physical alternative, electroporation remains one of the convenient strategies with translational potential to directly apply to the human body. Electroporation uses short electrical pulses to temporarily alter the permeability of the cell membrane and to trigger the subsequent cellular uptake of exogenous materials. The method has been reported for the successful delivery of various NA into cells or tissues (15). Robust humoral $CD4^+$ and $CD8^+$ T cell immune responses can be elicited by plasmid DNA vaccination using skin electroporation (16). However, conventional electroporation systems typically employ long and wide metal plates or clamp electrodes and require a prior injection of liquid vaccine formulation to the application site before electrical pulsing. Such multistep operation not only complicates the translational usage, but also affects the precision and controllability in the delivery of vaccine formulation (17, 18). Moreover, high voltage (>200 V) pulsing is often used, which could cause a high level of cell mortality and a strong sense of pain in human patients. There are also concerns regarding the instrumentation complexity and lack of scalability of conventional electroporation devices (19). Therefore, a painless, injection-free, one-step in vivo electroporation technique would be of great value for in vivo administration of NAs for immunotherapy applications.

Specifically oriented toward vaccination, transdermal delivery of vaccine materials to immune cells is a prerequisite. Recently, microneedle techniques have been developed as advanced drug delivery platforms for transdermal administration of different therapeutic reagents (20) and can also be used as an attractive alternative for minimally invasive immunotherapy, given the rich presence of professional antigen-presenting cells (APCs) and immune-accessory cells in subcutaneous regions that form a highly regulated immune network essential for effective vaccination (21, 22). Properly designed microneedles can mechanically penetrate the stratum corneum of skin to induce antigen-specific immune responses by delivery of vaccine materials (23). Ideally, such an operation can be self-administrated without causing pain or skin damage (24). Novel electroporation devices assuming a microneedle-based electrode were shown to improve the efficiency of transdermal gene delivery (25), which unveils the great clinical potential of the next generation of skin vaccination by combining electroporation, controlled biomolecule release, and minimally invasive transdermal access of immune cells. The integration of the microneedle with subcutaneous electroporation precisely controls the electrical pulses to transiently disrupt the cell membrane and thereby facilitates the direct and targeted delivery of vaccine materials (DNAs in this study) into the epidermal and dermal cells to improve the therapeutic outcome of the DNA vaccine, which is typically restricted due to low immunogenicity and insufficient cellular transfection (22, 26). The close and microscale contact of the microarrayed needle electrodes also allows the electroporation to be operated at a substantially lower voltage for better safety and cellular compatibility (27).

In this study, we develop μEPO devices for in vivo transdermal cytosolic delivery of NAs and microarrayed cell electroporation, which is specifically oriented toward one-step transfection of DNA vaccine in subcutaneous APCs for cancer immunotherapy. The μEPO device contains an array of microneedle-shaped electrodes with pre-encapsulated dry DNAs. Upon a pressurized contact with the skin tissue, the electrodes are rehydrated, electrically triggered to release DNAs, and then perform electroporation of nearby cells, which can achieve in vivo transfection of more than 50% in the epidermal and upper dermal layer. As a proof-of-concept, the μEPO technique is employed to facilitate transdermal delivery of neoantigen genes to activate antigen-specific immune response for enhanced cancer immunotherapy based on a DNA vaccination strategy. In an OVA cancer vaccine model, we show that high-efficiency transdermal transfection of APCs with OVA-DNAs induces robust cellular and humoral immune responses, including antigen presentation and generation of IFN-γ^+ cytotoxic T lymphocytes (CTLs) with a more than 10-fold dose sparing over existing IM injection approach, which effectively inhibited B16-OVA tumor growth in the animals. With the increasing prevalence of NA-based vaccines (28), it is expected the μEPO technique would offer a promising solution for one-step, self-administrable, and painless transdermal gene delivery in the clinical practice of immunotherapy.

Results

Design and Fabrication of the μEPO Device. The μEPO device was made of a conductive hydrogel, which is a composite of vinyl alcohol (PVA) and PEDOT:PSS, and is fabricated as an array of (10 × 10) microneedle electrodes by replicate molding. PVA was used to form the hydrogel scaffold matrix because of its unique properties in cross-linking structure, nontoxicity, biocompatibility, and swelling capability upon hydration (29); and PEDOT:PSS was used to render the material good conductivity (30). The microneedle format of the arrayed electrodes not only provides a solution for transdermal access, but also effectively improves the device performance of cell electroporation. The point discharge induced at the tip of the microneedle electrodes can significantly enhance the local electrical field, which would be sufficient to electroporate mammalian cells in a specific skin layer (27). With the current design, a μEPO device uses a substantially lower electroporation voltage (~30 V), which would otherwise be as high as 200 V in existing techniques (31). Besides working as the electroporator, the hydrogel electrodes also carry prepackaged biomolecules (e.g., DNA), which can be electrically triggered to be released via iontophoresis. Therefore, the single-component hydrogel-based electronic μEPO device performs multiple operations of a strategy for transdermal vaccination, including skin penetration, DNA injection, and in vivo cellular electroporation (Fig. 1).

Unlike the traditional metal-based electrodes, the hydrogel-based device fabrication is particularly advantageous in packaging NAs. In the current demonstration, the vaccine DNA was simply mixed with the hydrogel precursor solution before replicate molding, and the amount of loaded DNA can be easily tailored by adjusting its concentration in the precursor formulation. For optimized DNA release, the hydrogel microneedles were composed of two layers, which were formed by sequential molding with DNA-mixed or DNA-free hydrogel precursors. Only the tip part was loaded with DNA materials. The curing of the hydrogel was performed at room temperature by air drying. The whole process does not involve any organic solvent, heating treatment, or UV exposures, avoiding potential chemical or physical damage to the NAs. As shown in Fig. 2 *A*–*C*, the resulted hydrogel electrodes exhibited a pyramidal shape with a 10 μm wide tip. Each microneedle electrode has a height of ~930 μm, a base width of ~380 μm and a center-to-center spacing of ~740 μm. The hydrogel patch with the microneedle electrodes was directly fixed on a copper pad and then mounted on an adhesive medical tape to form a functional μEPO device, which could be applied to human skin for therapeutic usage (Fig. 2 *D*–*F*).

To test the structural stability of the μEPO device, thermogravimetric analysis (TGA) was conducted. The results showed that the inclusion of PEDOT:PSS improved the overall stability of the PVA-based hydrogel electrodes, which is attributed to the elevated polymer degradation temperature from 260 °C to 423 °C (*SI Appendix*, Fig. S1). Mechanical analysis was performed to evaluate the device's capability to penetrate skin tissue. The average

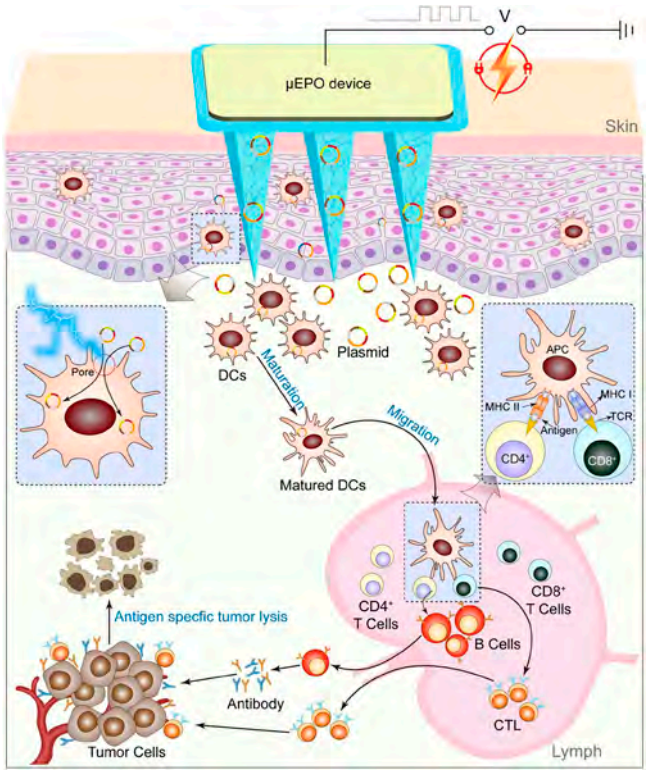

Fig. 1. Schematic of transdermal microarrayed electroporation for enhanced cancer immunotherapy based on DNA vaccination. The arrayed hydrogel electrodes encapsulating DNAs are employed for both highly efficient transdermal gene delivery and in vivo cell electroporation. Subcutaneous dendritic cells (DCs) are transfected with neoantigen genes and are homed to lymph nodes to activate T cells, eliciting robust humoral and cellular response for enhanced cancer immunotherapy.

failure force was measured to be 0.4 N/needle, which was sufficient to puncture through human skin without breaking (32) (Fig. 2*G*). The penetration capability of the μEPO electrodes was further validated for effective puncturing of the porcine skin for subcutaneous access without breaking afterward (*SI Appendix*, Fig. S2). The hydrogel electrodes showed excellent conductivity of 1.93 ± 0.71 S/m (Fig. 2*H*). When a dry device was rehydrated in PBS, the microneedle electrode swelled with a ~50% volume increase in 10 min (Fig. 2*I*). The rehydration and swelling were slightly less when μEPO device was applied to a mouse skin (*SI Appendix*, Fig. S3*A*), but still fast enough to ensure the efficient release of biomacromolecules upon a low-voltage stimulation.

Low-Voltage-Driven Release of NAs. To study the electrically controlled release of biomolecules from a μEPO device, DNA plasmids encoding the OVA gene were packaged in the hydrogel electrodes, which were inserted into a block of agarose gel to mimic their interfacing with skin tissue. Application of a negative potential across the microneedle electrode could drive the release of negatively charged DNAs by iontophoresis (33). The releasing kinetics were quantitatively evaluated by analyzing the DNAs in a block of agarose, which was used to emulate the μEPO–tissue interface. The number of released DNAs was closely correlated with the amplitude and duration of the applied electrical stimulation. At a fixed duration of 10 min, the releasing amount showed a positive correlation with increasing voltage up to 1.0 V (Fig. 2*J*). At a fixed voltage stimulation of 1.0 V, the release also increased monotonically with a longer stimulation period, and 1,964 ± 40 ng OVA DNAs were released to the agarose within 10 min (Fig. 2*K*). Similar release kinetics are also observed for eGFP DNA plasmids (*SI Appendix*, Fig. S3*B*). While some passive leakage of DNAs could also happen due to the porous structure of the conductive hydrogels, the voltage-driven release was found to be threefold higher than that from passive diffusion. This feature not only overcomes the technical limitations to improve DNA translocation from hydrogel packages, but also provides a controlled release mechanism for highly efficient in vivo cellular transfection applications. This is particularly beneficial for in vivo electroporation, where the timing and amount of DNA available in the proximity of target cells are crucial for achieving high-efficiency transfection. In the context of DNA vaccination and gene therapies, the controlled delivery of nucleic acid materials could subsequently enhance the induced immune response or therapeutic efficacy (34).

Electrical Field Characterization. To characterize the electrical field generated by a μEPO device for electroporation purposes, we first performed a numerical simulation to study the electrical field distribution when a device is engaged for transdermal gene delivery. A low-voltage case and a high-voltage case were evaluated to analyze the condition for driving DNA release or for inducing cellular electroporation, respectively. In the current configuration, the intensity of electrical field was dramatically enhanced around the tip of the microneedle electrodes, where their morphology is known to affect the intensity of the electrical field (35). For the low-voltage case, the electrical field was moderately strengthened around the electrode tips, which is sufficient to induce iontophoresis for DNA release (Fig. 2*L*). For the high-voltage case, a 90 V electrical pulsing was able to induce an electrical field over 400 V/cm in close proximity to the electrode tips, which would be the threshold field intensity for efficient cell electroporation (36). The strong electrical field showed a limited spatial extension (Fig. 2*M*), so that only cells in the epidermis and upper layer of the dermis are affected. The abundant existence of APCs (e.g., Langerhans cells) in these regions would be the target for modulating human immune response (23). It was not surprising to see a close correlation between the electrical field and voltage stimulation (*SI Appendix*, Fig. S4), a balanced optimization of the electrical pulsing amplitude, duration, and effective range was achieved by using 90 V for electroporation. At the same voltage used for electroporation (10 pulse, 50 ms/pulse), significantly lower DNA was released than the case using continuous low-voltage stimulations for dedicated driving of DNA release. But the later electroporation also showed a beneficial synergy (*SI Appendix*, Fig. S5) for transdermal vaccination that requires subcutaneous DNA release for in vivo cellular transfection. It is worth noticing that continuous high-voltage stimulation (90 V) could induce electrolysis of the biological solution surrounding the hydrogel electrodes, emphasizing the importance of using a continuous low voltage (1 V) for confirmed efficacy and safety of the μEPO device.

Microarrayed Electroporation for Efficient Intracellular Gene Delivery. Using an ex vivo model, the μEPO device was then evaluated for its efficiency of intracellular gene delivery by microarrayed cell electroporation. Gelatin methacryloyl (GelMA)-based hydrogel was used to prepare an extracellular matrix for 3D culture of HEK293T cells, on which a μEPO device was applied to emulate the configuration of transdermal electroporation for DNA transfection. A sustained low-voltage stimulation and a high-voltage pulsing were applied sequentially to trigger DNA release and to perform electroporation, respectively (Fig. 3*A*). Live/dead staining was performed afterward to demonstrate the safety of the device and operation. The cell viability was more than 90%, showing no difference in comparison to untreated samples

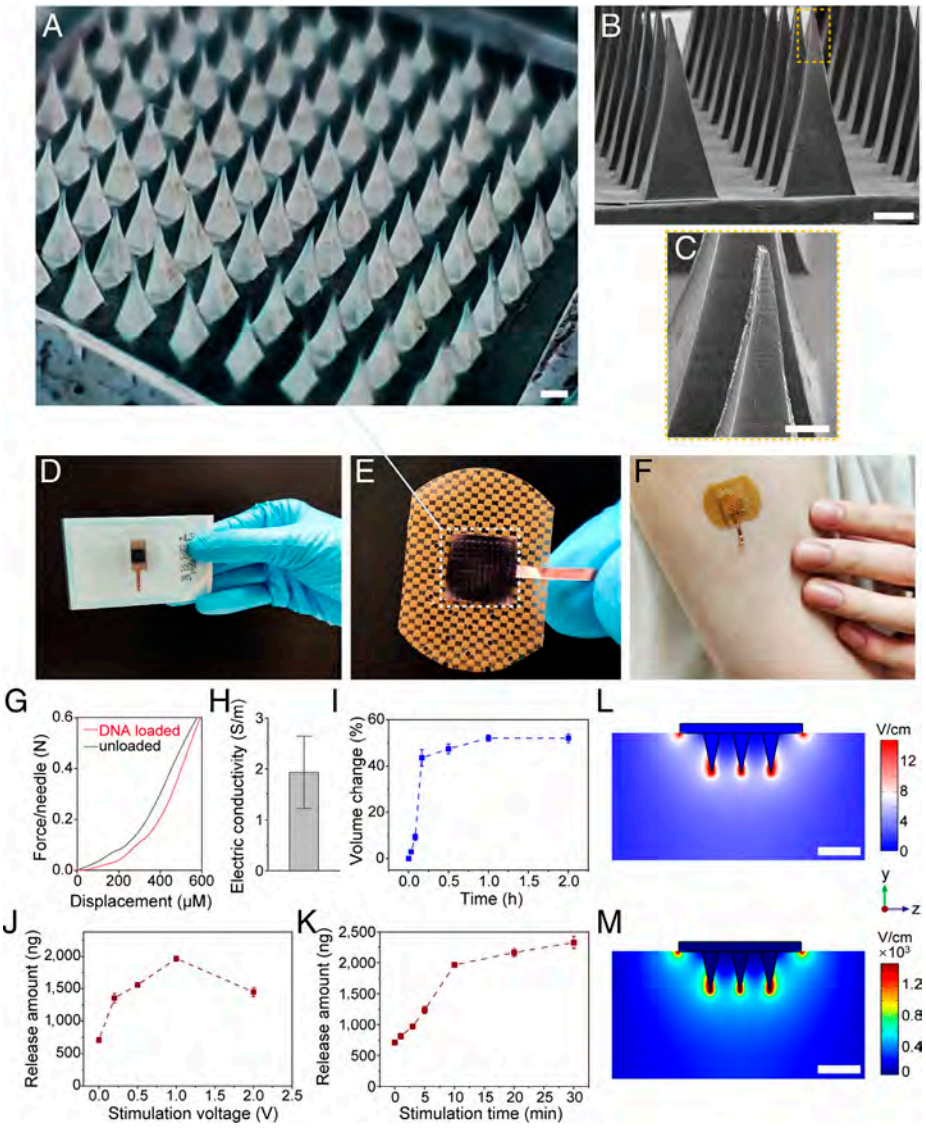

Fig. 2. Fabrication and characterization of the μEPO device. (*A*) Optical image of the DNAs-loaded hydrogel electrode array on a μEPO device. (Scale bar, 200 μm.) (*B*) Scanning electron microscopy (SEM) image of the electrodes. (Scale bar, 200 μm.) (*C*) Magnified SEM image showing the tip of a hydrogel electrode outlined in panel (*B*). (Scale bar, 100 μm.) (*D* and *E*) Photographs of packaging and mounting a μEPO device on an adhesive tape. (*F*) An illustrative application of a μEPO device on the human arm. (*G*) Mechanical analysis of the μEPO device with or without DNA loading (OVA plasmids, n = 3). (*H*) Conductivity characterization of the μEPO device (n = 3). (*I*) Measurement of the volume swelling of the μEPO device (n = 3). (*J* and *K*) Controlled release of DNAs (OVA, 10 μg load) from the μEPO device as functions of stimulation voltage (*J*) and duration (*K*). (*L* and *M*) Numerical simulation of electrical field distribution at around individual hydrogel electrodes with low (1 V) and high (90 V) voltages. (Scale bar, 1 mm.) Data are presented as mean ± SEM.

(Fig. 3 *B* and *C*), suggesting good biosafety of the μEPO device and associated operations (*SI Appendix*, Fig. S6).

It is known that electroporation facilitates intracellular gene delivery by transiently interrupting the cell membrane for DNAs to enter. μEPO's capability to disrupt the cell membrane was first evaluated by intracellular delivery of fluorescent molecules (FITC-dextran, 3 to 5 kDa, 1 μg) to the 3D cultured HEK293T cells. Within ~250 μm from the microneedle electrode penetrated micropores, the results showed more than 80% of the cells were loaded with the fluorescent molecules, which was significantly higher than that observed from the control group (Fig. 3 *D* and *E*), suggesting a successful and viable disruption of the cell membrane by the microarrayed electroporation. We next examined intracellular delivery of eGFP DNA using a μEPO device loaded with 10 μg plasmid per patch. Successful eGFP expression was observed in about 60% of the cells, which was quantified by confocal microscopy (Fig. 3*F* and *SI Appendix*, Fig. S7) as well as by flow cytometry (Fig. 3 *G* and *H*). These ex vivo results show that the μEPO enables efficient intracellular gene delivery by performing microarrayed DNA delivery and cell electroporation.

In Vivo Transdermal Gene Delivery. Transdermal gene delivery was evaluated in a mouse model by applying the μEPO device on its shaved skin through a thumb-pressing process (*SI Appendix*, Fig. S8). A platinum electrode was engaged oppositely as the ground electrode, and a negative voltage was applied to the μEPO device to trigger the release of plasmid and in vivo electroporation (Fig. 4*A*). The transdermal molecule delivery was initially assessed by in vivo delivery of FITC-dextran (3 to 5 kDa), which was analyzed by direct in vivo imaging 30 min after μEPO application (Fig. 4 *B* and *C*). The success in transdermal delivery of FITC-dextran into individual cells was further confirmed by imaging of stained tissue sections (*SI Appendix*, Fig. S9). Then, the μEPO device was used to perform transdermal transfection of eGFP DNA transfection. After a pressured contact with skin, a low-voltage (1 V) driven release of the DNAs and a high-voltage (90 V) driven electroporation were performed sequentially to achieve effective transdermal gene delivery. Twenty four hours later after electroporation, the eGFP expression in the epidermis and upper dermis was quantified by confocal imaging of extracted skin tissues, which showed more than one order of magnitude higher transfection efficiency at the application site, in comparison to the controls (Fig. 4 *D* and *E*). The statistic eGFP fluorescence intensity showed at least fourfold improvement at the electroporation site (Fig. 4*F*). The minimal invasiveness of the treatment was evidenced by a quick recovery of the sign of pressured contact after electroporation, no visually detectable skin damage was observed. The sign of skin puncture by the

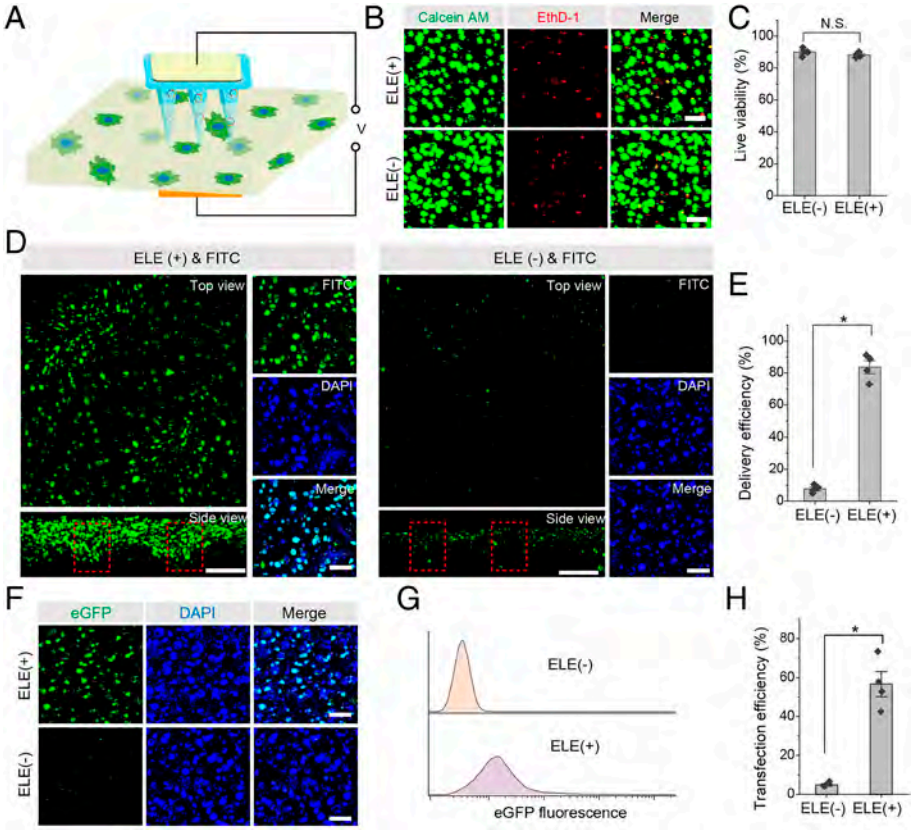

Fig. 3. Ex vivo characterization of microarrayed electroporation for intracellular gene delivery. (*A*) Schematic of the ex vivo model. (*B*) Fluorescence images showing live (green, Calcein AM) and dead (red, EthD-1) cells in a cell-laden hydrogel with [*Top* panel, ELE (+)] and without [bottom panel, ELE (−)] microarrayed electroporation. (Scale bars, 100 μm.) (*C*) Quantification of cell viability after μEPO treatment (n = 4). (*D*) 3D confocal images of intracellular FITC-dextran delivery using a μEPO device with [ELE (+)] or without [ELE (−)] electroporation. The regions of electrode insertion are indicated by red boxes. (Scale bars, 200 μm.) Enlarged views are shown on the right. (Scale bars, 100 μm.) (*E*) Quantification of delivery efficiency (n = 4). (*F*) Confocal images showing eGFP-DNA transfection in 3D culture of HEK293T cells with [ELE (+)] or without [ELE (−)] microarrayed electroporation. (Scale bars, 100 μm.) (*G* and *H*) Representative flow cytometry data and statistical data showing eGFP-DNA transfection efficiencies (n = 4). Data are presented as mean ± SEM, * indicates $P < 0.05$, N.S., not significant, by Student's *t* test.

microscale electrodes was observed immediately after treatment, gradually faded away within 10 min, and completely disappeared after 30 min (Fig. 4*G* and *SI Appendix*, Fig. S10*A*). Histological sectioning of treated skin tissues showed a uniform pattern of electrode insertion into the epidermis layer without disruption of underlying dermal layers of capillary vessels (Fig. 4*H*), and no significant increase of inflammatory response was observed 24 h after μEPO treatment (*SI Appendix*, Fig. S10*B*). These results suggested good biocompatibility and safety of the μEPO platform.

Immune Response Induced by μEPO-Facilitated DNA Vaccination. After confirmation of successful transdermal DNA delivery to cells in the epidermis and upper dermis, the μEPO device was then formulated with DNAs encoding OVA antigen, which was designed to induce immunogenicity response after being transfected to epidermis cells using μEPO facilitated in vivo electroporation (Fig. 5*A*). Transgenic melanoma cells that express OVA antigens (a pseudotumor antigen) provide a convenient way to study cancer vaccines (37). The treated skin tissues were first evaluated 2 d later to examine neoantigen (OVA) expression, which showed a transfection efficiency over 60% throughout the epidermis (Fig. 5 *B*–*D* and *SI Appendix*, Fig. S11*A*). We leverage specific antibodies to detect and visualize the colocalization of OVA protein in $CD11c^+$ APCs in treated subcutaneous regions, given their pivotal role in eliciting adaptive immune response. More dendritic cells (DCs, $CD11c^+$) were recruited to the application site, among which a significant portion (84.5 ± 4.3 %) were cocolocalized with OVA expression (Fig. 5*B* and *SI Appendix*, Fig. S11 *B* and *C*). Further examination of cryosectioned skin after 7 d showed a sustained antigen expression and antigen presentation (*SI Appendix*, Fig. S12). These results suggested success in transfecting DCs with desired antigen gene, which is a crucial step to antigen presentation and initiation of subsequent antigen-specific immune response (38).

In immunized C57BL/6 mice, we then analyzed the draining lymph node (dLNs) 7 d after transdermal gene delivery (OVA-ELE, 10 μg/patch). For a comprehensive evaluation of the efficiency, we included extensive control groups for benchmark comparison, including intramuscular injection of OVA-DNAs (IM), intramuscular injection of lipofectamine plus OVA-DNAs formation (Lipo), intramuscular injection of DNAs plus bulk electroporation (IM-bEP), subdermal injection of OVA-DNAs plus bulk electroporation (SD-bEP), along with OVA-DNAs free μEPO device (ELE) and OVA-DNAs loaded μEPO device but no electrical stimulation (OVA). The mice were immunized with an OVA-DNAs-loaded μEPO device (OVA-ELE) or the control formulations using equivalent doses of OVA plasmid DNAs. As an indication of the elicited adaptive immune response, the dLNs and peripheral blood mononuclear cells (PBMCs) were examined 7 d postvaccination. Mice vaccinated with OVA-DNAs by μEPO showed a significant increase in $CD80^+$ and $CD86^+$ double-positive DCs (38.64 ± 1.36%) in the dLNs (Fig. 5 *E* and *F*). The OVA-ELE group also resulted in a significantly elevated level (5.04 ± 0.23%) of $CD11c^+$SIINFEKL-H-2 Kb^+ antigen cross-presented DCs (Fig. 5*G*). Also, the OVA-ELE immunized mice showed significant enrichment of activated DCs ($CD11c^+CD86^+$ or $CD11c^+CD80^+$, *SI Appendix*, Fig. S13 *A* and *B*). In addition, the OVA-ELE vaccination induced a higher level of DCs maturation and cross-presentation than the results acquired from animals receiving IM vaccination at much higher doses (100 μg) (*SI Appendix*, Fig. S13 *C* and *D*). After three vaccination shots, we further observed a higher level of $CD11c^+CD80^+CD86^+$ DCs and $CD11c^+$SIINFEKL-H-2 Kb^+ antigen cross-presenting cells (*SI Appendix*, Fig. S14), which is consistent with a previously reported vaccination (39).

Mature DCs are known to initiate T cell–mediated immune responses (29). Next, we proceeded to examine the induction of cytotoxic T lymphocytes (CTLs) response by the μEPO facilitated transdermal gene delivery. Circulating peripheral blood

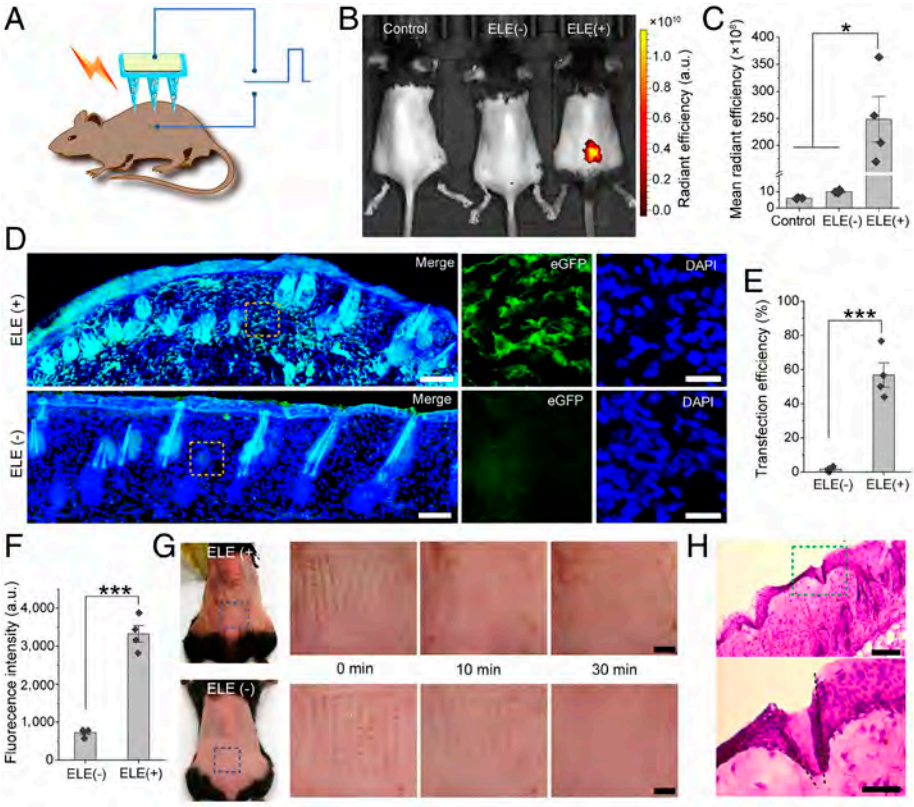

Fig. 4. μEPO-facilitated in vivo transdermal gene delivery. (*A*) Schematic of the experimental design. (*B* and *C*) In vivo images and statistical data showing subcutaneous delivery of FITC via mouse skins. (*D*) Stitched fluorescent images showing subcutaneous eGFP-DNA expression in μEPO-treated mice. (Scale bars, 100 μm.) Orange squares indicate the area penetrated by a hydrogel electrode. (Scale bars, 25 μm.) (*E* and *F*) Quantitation of transfection efficiency (*E*) and fluorescence intensities (*F*) showing subcutaneous eGFP-DNA expression at the application sites. (*G*) Skin recovery after applying a μEPO device on mouse skins. (Scale bars, 1 mm.) (*H*) Hematoxylin and eosin (H&E) staining images of μEPO-treated skin showing epidermal disruption at the insertion sites. (Scale bar, 300 μm (*Top*); 100 μm (*Bottom*).) The control groups include untreated animals and mice treated by μEPO with [ELE (+)] and without [ELE (−)] electroporation, n = 4, data are presented as mean ± SEM, * indicates $P < 0.05$, *** indicates $P < 0.001$ by Student's *t* test.

mononuclear cells (PBMCs) were analyzed 7 d after in vivo transfection of OVA-DNAs. The frequency of SIINFEKL-MHC-I tetramer$^+$CD8$^+$ cells showed a multifold increase in the OVA-ELE group (2.96%) over the control groups (untreated 0.42%, ELE 0.47%, OVA 0.64%, IM 0.82%, and Lipo 0.65%, Fig. 5*H*). The μEPO immunized mice (OVA-ELE) also showed a remarkable increase in IFN-γ$^+$ (1.87 ± 0.13 %), which is an 18-fold enrichment over the untreated group ($P < 0.0001$) or a nearly twofold increase over the IM injection group ($P = 0.008$, 10× dose,100 μg DNA), suggesting at least a 10-fold dose sparing enabled by using the μEPO device (Fig. 5*I* and *SI Appendix*, Figs. S15 and S16). The enrichment of IFN-γ$^+$ CTLs was quite significant and is comparable to recently published vaccination systems based on nucleic acid materials (40, 41). Particularly, it was clearly observed that the OVA-ELE group showed the best performance in all aspects of the analysis, which was significantly better than the Lipo or IM-bEP groups for the level of CD80$^+$CD86$^+$ DCs (Fig. 5 *E* and *F*), the percentage of OVA (SIINFEKL)-presenting DCs (Fig. 5*G*), the enrichment of antigen-specific CD8$^+$ T cells in peripheral blood (Fig. 5*H*), and the induction of a CTL response (Fig. 5 *H* and *I*).

Upon restimulation with OVA antigen, the splenocytes collected from OVA-ELE mice secreted much higher levels of IFN-γ than those collected from mice in the negative control groups (Fig. 5*J*). To evaluate the antigen-specificity of the enhanced immune response, splenic T lymphocytes extracted from vaccinated mice were cocultured with B16-OVA cancer cells, and the cytotoxic activity of these CTLs was quantitatively measured in vitro using a lactate dehydrogenase (LDH) release assay. The effector lymphocytes isolated from OVA-ELE mice showed the highest CTL killing capacity by inducing specific lysis of B16-OVA cancer cells (Fig. 5*K*). Multiple μEPO-facilitated DNA vaccination continued to enhance the antigen-specific T cell mediated immune responses (*SI Appendix*, Fig. S17), without causing toxicity in all major organs, including the liver, kidney, lung, heart, and spleen (*SI Appendix*, Fig. S18). These results demonstrate the efficacy of our μEPO technique by achieving a high transfection efficiency in APCs, promoting dendritic cell maturation, and inducing a robust CTL response. While the μEPO treatment exhibited slight improvement over the SD-bEP group, the painless and minimally invasive operation still justifies the unique advantages of the μEPO technique to facilitate transdermal DNA vaccination procedures.

Inhibition of Tumor Growth in Vaccinated Animals. With the capability to stably induce antigen-specific immune response, we then proceeded to evaluate the antitumor efficacy of μEPO-facilitated OVA-DNAs vaccination. For different treatment groups (OVA-ELE, OVA, ELE, and IM), a prophylactic strategy was experimented with using B16-OVA tumor-bearing mice (Fig. 6*A*). Healthy C57BL/6 mice received three shots of OVA-DNAs before tumor inoculation. OVA-ELE immunized mice showed the most significant tumor regression (*SI Appendix*, Fig. S19). The tumor size (395.6 ± 205 mm^3 and 0.14 ± 0.08 g) was considerably smaller than those observed in other groups (e.g., 830 ± 218.5 mm^3 and 0.6 ± 0.17 g in the IM group, Fig. 6 *B*–*D*). Accordingly, the survivals of OVA-ELE immunized mice were significantly prolonged (Fig. 6*E*).

Next, we assessed the T lymphocyte infiltration of tumor tissues 10 d after tumor inoculation. The tumor-infiltrating lymphocytes (TILs, CD3$^+$ T cells, and CD4$^+$ T cells) were significantly increased in the tumors extracted from OVA-ELE animals (*SI Appendix*, Fig. S20 *A* and *B*). Compared to untreated animals, about 26-fold increase of CD8$^+$ cells was observed in OVA-ELE mice, while only a 4.8-fold increase was observed in animals receiving IM of OVA-DNAs (Fig. 6*F* and *SI Appendix*, Fig. S20*C*). The proportion of CTLs (CD3$^+$CD4$^-$CD8$^+$) and effector T cells (CD3$^+$CD4$^+$CD8$^-$) within the tumors were also significantly increased in the OVA-ELE group (Fig. 6 *G* and *H*). In the CD3$^+$ cells that infiltrated the tumors, the percentage of CD8$^+$ cells was

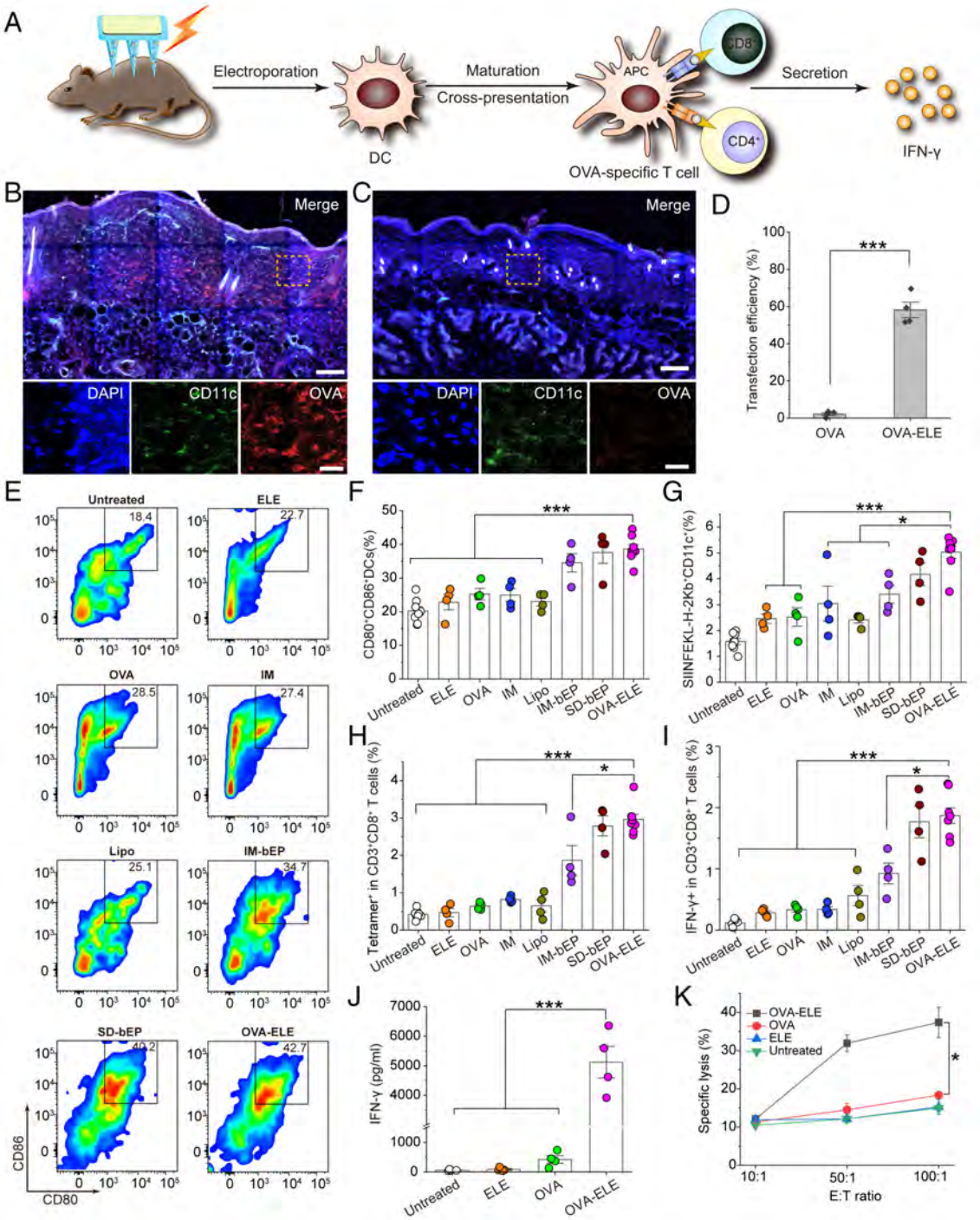

Fig. 5. Immune response induced by μEPO-facilitated transdermal DNA vaccination. (*A*) Schematic of the experimental design. (*B* and *C*) Stitched fluorescent images showing the expression OVA in subcutaneous DCs ($CD11c^+$) 48 h after μEPO-facilitated transdermal delivery of OVA-DNAs. (Scale bars, 100 μm.) The boxed regions are enlarged at *Bottom* panels. (Scale bar, 25 μm.) (*D*) Quantitation of transfection efficiencies. (*E* and *F*) Representative flow cytometry data (*E*) and statistics (*F*) showing in vivo DCs maturation. (*G*) Proportions of $CD11c^+SIINFEKL^+$ SIINFEKL-presenting DCs in the draining lymph nodes (dLNs). (*H*) The percentage of the H-2 Kb/SIINFEKL tetramer staining of $CD3^+CD8^+$cells in peripheral blood mononuclear cells (PBMCs). (*I*) The frequency of IFN-γ positive cells in $CD3^+CD8^+$ cells from restimulated PBMCs. (*J*) IFN-γ secretion of splenocytes in the culture supernatants after restimulation with OVA antigen for 72 h. (*K*) In vitro killing capacity showing the percentage of the lysis of target B16-OVA cells at different E/T ratios. "E", effector lymphocytes; "T", target B16-OVA cells. The immune responses are evaluated 7 d postimmunization. Data are presented as mean ± SEM, n = 4 to 8 (8 for OVA-ELE and untreated group, 4 for other groups), * indicates $P < 0.05$, *** indicates $P < 0.001$ by Student's *t* test.

also substantially increased, which was reported to benefit antitumor therapy (41) (Fig. 6*I*).

Treating Cancer with Transdermal Delivery of OVA Gene. Besides working as a DNA vaccination strategy, the μEPO-facilitated transdermal delivery of the OVA gene can also be developed as a therapeutic cancer treatment. In this study, this strategy was further examined in animals receiving tumor inoculation 5 d before in vivo transfection of OVA-DNAs (Fig. 7*A*). While it was observed that simple transdermal introduction of OVA-DNAs (e.g., IM or diffusion leakage in OVA groups) can mildly slow down the tumor growth, triple transdermal transfection of OVA

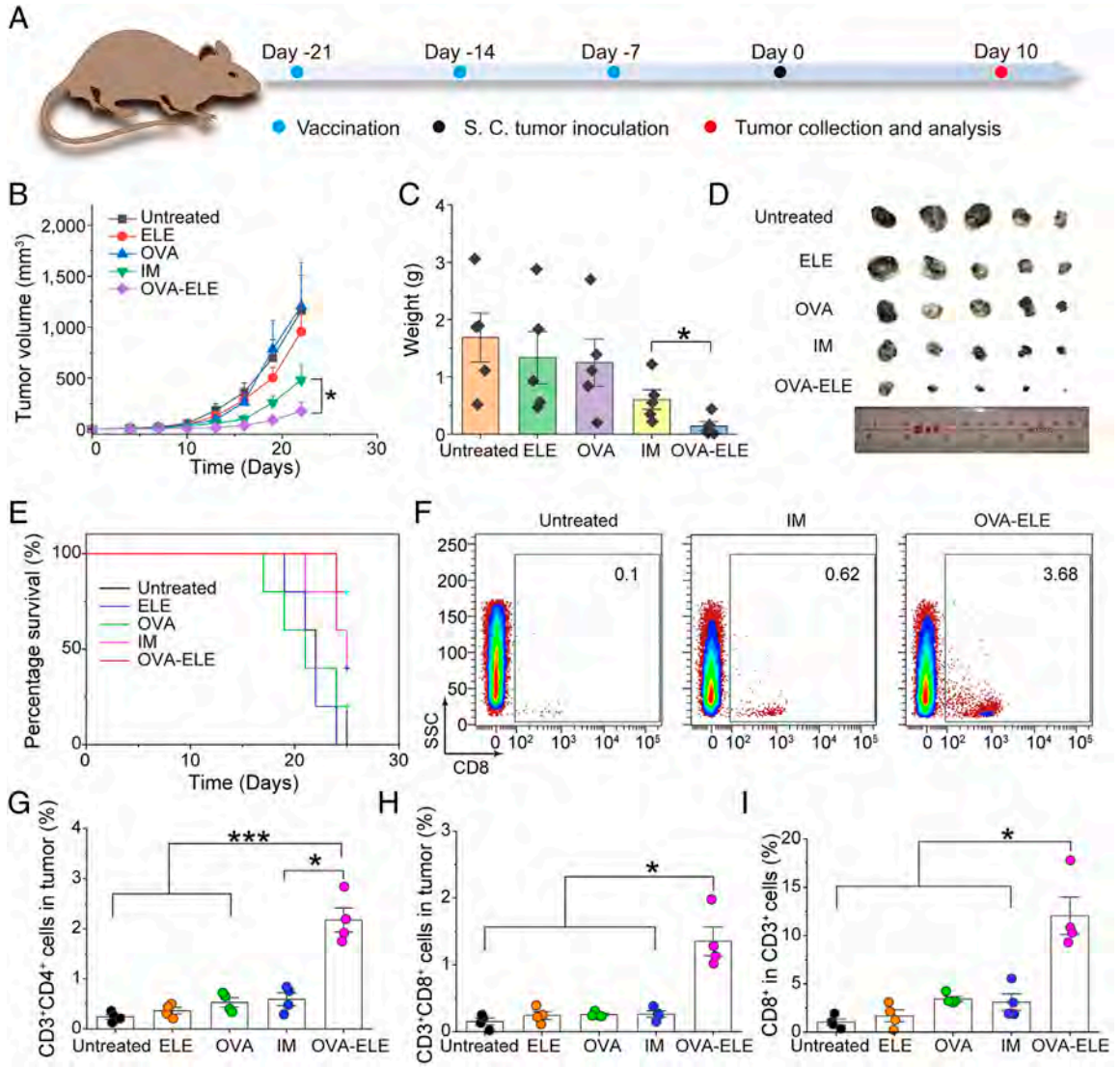

Fig. 6. Inhibition of tumor growth in vaccinated animals. (*A*) Schematic illustration of prophylactic cancer effect of the μEPO-facilitated transdermal DNA vaccination. (*B*) Average tumor growth curves of the B16-OVA tumors on mice after vaccination (OVA-ELE, n = 5). (*C*) Weights and (*D*) sizes of tumors excised from different experimental groups (n = 5). (*E*) The Kaplan–Meier survival curves (n = 5). (*F*) Representative flow cytometry analyses of $CD8^+$ T cells in excised tumors. (*G–I*) Quantification analyses of intertumoral (*G*) $CD3^+CD4^+$ and (*H*) $CD3^+CD8^+$ T cells (n = 4). (*I*) Portion of $CD8^+$ cells out of $CD3^+$ cells (n = 4). The analysis was performed 10 d after tumor inoculation. The control groups include untreated animals (Untreated), DNA-free μEPO with electroporation (ELE), DNA-loaded μEPO without electroporation (OVA), and intramuscular injection (IM). Data are presented as means ± SEM, * indicates $P < 0.05$, *** indicates $P < 0.001$ by Student's *t* test.

gene by using μEPO achieved significantly stronger inhibition of tumor growth (Fig. 7 *B* and *C* and *SI Appendix*, Figs. S21 and S22), leading to substantially smaller tumors in OVA-ELE animals. The survival of OVA-ELE mice was significantly prolonged (Fig. 7*D*). At a cellular level, we found significantly more infiltration of T cells in the tumor isolated from OVA-ELE animals (Fig. 7 *E–G*). The population of infiltrating $CD3^+$, $CD4^+$, and $CD8^+$ T cells was increased by more than 23-fold, 17-fold, and 15-fold in comparison to the untreated group, respectively; the percentage of both $CD3^+CD8^+$ and $CD3^+CD4^+$ T cells within tumors was also significantly increased in the OVA-ELE group (*SI Appendix*, Fig. S23), and the percentage of Tregs cells ($CD4^+Foxp3^+$) was significantly decreased in the OVA-ELE group (Fig. 7*H*). Moreover, the serum levels of cytokines (IFN-γ) in OVA-ELE mice were significantly increased when compared with the control groups (Fig. 7*I*), which contributes to the anticancer efficacy by antigen-specific activation of the immune response. Taken together, these results suggest that, even after cancer induction, in vivo transdermal transfection of OVA-DNAs can work as a therapeutic tool to treat cancer.

Discussion

This study presented an organic electronic device for in vivo gene delivery by transdermal microarrayed electroporation, which overcomes the challenges of inefficient delivery of macrobiomolecules (e.g., proteins, NAs) in existing immunotherapies (5). The multifunctional organic device (μEPO) was made of conductive hydrogels, which were fabricated into microneedle-shaped electrodes to work as an electrical biointerface and a molecule carrier for one-step transdermal gene delivery, combining controlled macromolecules release, in situ electroporation, and in vivo gene-transfection in a trinity. Our results demonstrate that the μEPO device enables a convenient, safe, and effective transdermal gene delivery platform to facilitate a highly efficient expression of DNAs in epidermic cells, including APCs, which is sufficient to induce antigen-specific immune response for immunotherapy of cancer in rodent animal model.

For an organic device based on hydrogel electronics, the preparation of a μEPO device does not involve any complex fabrication processes as typically used in MEMS devices (42) and can be

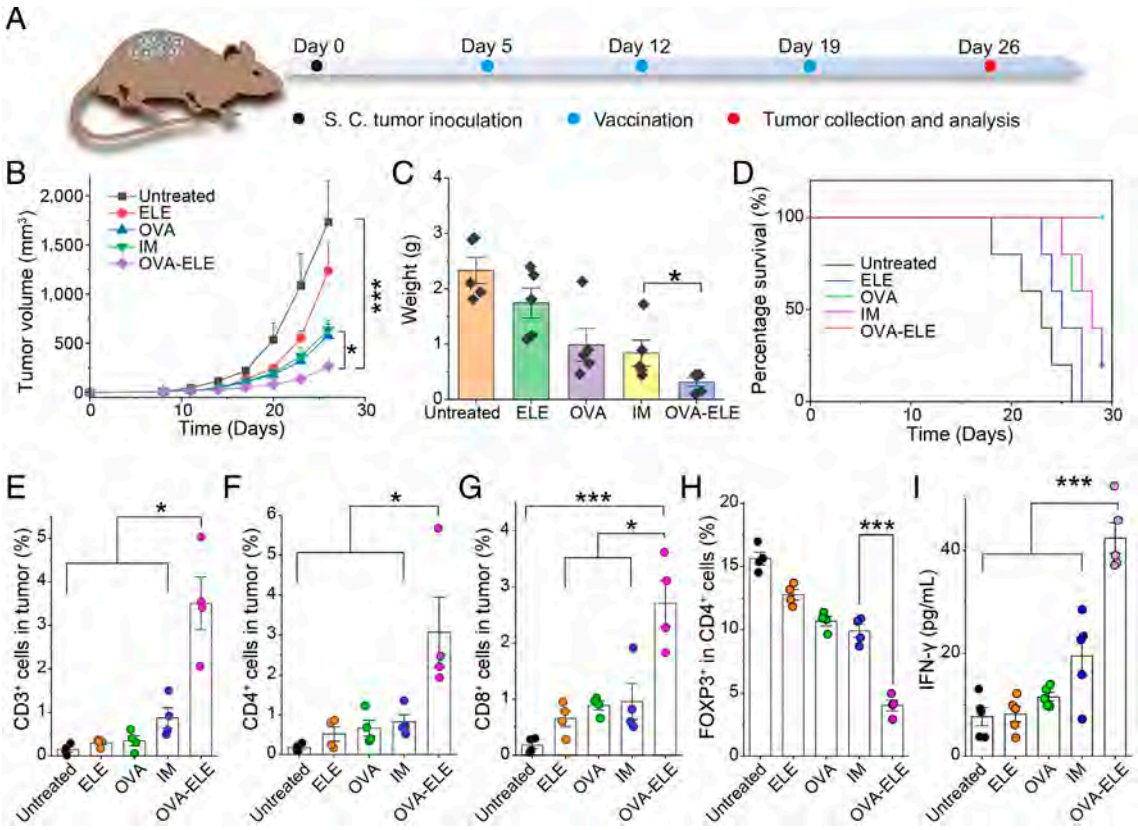

Fig. 7. Treating cancer with transdermal delivery of OVA-DNAs. (*A*) Schematic illustration of therapeutic treatments for inhibiting the B16-OVA tumor growth. (*B* and *C*) Evaluation of tumor growth in (*B*) average growth curves and (*C*) weights for different experimental groups (n = 5). (*D*) Kaplan–Meier survival curves for various treatments (n = 5). (*E*–*H*) Quantification analyses of intertumoral (*E*) $CD3^+$ T cells, (*F*) $CD4^+$ T cells, (*G*) $CD8^+$ T cells, and (*H*) $Foxp3^+$ portion in $CD4^+$ cells (n = 4). (*I*) IFN-γ concentrations in the serum of the treated mice (n = 5). The analysis was performed 7 d after three consecutive treatments. The control groups include: untreated animals (Untreated), DNA-free μEPO with electroporation (ELE), DNA-loaded μEPO without electroporation (OVA), and intramuscular injection (IM). Data are presented as means ± SEM, * indicates $P < 0.05$, *** indicates $P < 0.001$ by Student's *t* test.

performed simply by a replicate molding using mixed precursor containing three major components (i.e., PVA, PEDOT:PSS, and target macromolecules). The convenient preparation allows flexible molecule packaging and precise dose adjustment, based on practical consumption in therapeutic treatment. Particularly, the well-controlled molecule release under skin tissue can be regulated by a first phase of low-voltage (0.2 to 1 V) electrical stimulation, thus avoiding unexpected overdosing that may cause systemic toxicity or inflammatory response for NA delivery. Particularly, after DNA packaging, the μEPO device is stored in dried status till usage (*SI Appendix*, Fig. S24). The DNA-loaded hydrogel electrodes would remain bioactive and get rehydrated upon reaching the epidermal tissue after penetrating the skin surface. This feature would substantially benefit the storage and transport of biologic therapeutics, which would be especially critical for point-of-care usage or wide application in underdeveloped regions (28).

As known, the skin barrier precludes topical delivery of most macromolecules, especially the charged ones (10). The μEPO device can break the barrier by penetrating the stratum corneum, followed by a voltage-driven release and in situ electroporation. For transdermal delivery, the microneedle-shaped electrodes on a μEPO device are specifically designed to facilitate molecule transport to tissues under skin surface, which effectively replaces the function performed by syringe injection in most existing clinical practice. Even for a recently reported metal-based in vivo electroporation system (25), NAs are still required to be injected separately. It has been widely reported that microneedles below 1 mm in length are used to painlessly pierce the stratum corneum and penetrate the human epidermis layer at an appropriate depth without stimulating pain-associated nerves (43). The use of microneedle patches in long-term drug delivery, such as insulin and hormone, has been reported as the major painless solution for transdermal applications (44, 45). Practically, microneedle structure has also been integrated into various clinical products to enhance the comfort and efficacy of transdermal drug delivery (46). In this project, careful consideration has been given to the device design and application procedures to achieve "painless" treatment while ensuring optimal treatment efficacy. By using a μEPO device, charged macromolecules can be delivered through the skin and then into the intracellular domain for cells around the device, accommodating a one-step DNA vaccination strategy without the need of any chemical transfecting reagents (e.g., lipid-like materials) (7, 18), which could otherwise be cytotoxic or cause unexpected allergic symptoms in human recipients, thus accommodating a footprint-free transdermal NA delivery.

Additionally, the "footprint-free" concept is also manifested by the fact that the conductive hydrogel-based μEPO device does not leave any degraded chemical molecules behind after the vaccination procedures. Particularly, the device was removed immediately after the electroporation process, and the whole process lasted around 11 min. Given the short contact time, the likelihood of hydrogel molecule leakage into the bloodstream is minimal. Because of the strong hydrogen bonds formed between the hydroxyl group in PVA and the sulfonate group in PEDOT: PSS, the conductive molecules can be locked in the inner structure of the hydrogel matrix to render structural stability, thus reducing the risk of molecule leakage during the short operation period (*SI Appendix*, Fig. S25).

Along with a topical delivery, the μEPO platform is also helpful in reducing systemic side effects and potential allergy cases, when compared to oral, parenteral, or intramuscular administrations. Besides the capability to penetrate the skin surface, it is also critical for biologic therapeutics to access the intracellular region of human cells, especially when RNAs or DNAs are intended to be used for vaccination purpose. Toward this goal, the μEPO technique enables a microarrayed in vivo electroporation, which has been shown to achieve highly efficient and safe intracellular delivery of different molecules both in vitro and in vivo, with an improvement of transfection efficiency of at least 10 folds over the control group and keeping 90% of the cells viable. It is known that different cell populations exist in these skin layers. The epidermis primarily comprises keratinocytes and Langerhans cells (a subset of dendritic cells), while the dermis is enriched with fibroblasts, dermal dendritic cells, and macrophages (21). Generally, the μEPO system employs a mechanical approach to breach the stratum corneum, facilitating intracellular delivery into the epidermis and upper dermis (Fig. 4*D*). Such delivery is not selective to cell types, it is likely that cells in proximity of the hydrogel electrodes are transfected with certain probability, and a mixed cell populations would be affected. As we observed, a significant majority, exceeding 60% of cells nearby the electrodes expressing OVA antigen in the epidermis (Fig. 5*D*). Particularly in this study, the magnitude of the immune response elicited by vaccine administration is primarily influenced by the transfection of APCs within the target tissue. Upon antigen expression or uptake, APCs undergo rapid maturation and migrate to the local draining lymph node where antigens are presented to T cells or B cells to initiate the humoral or cellular immune response to prevent and control viral infection or kill tumor cells (34). Therefore, we specifically targeted $CD11c^+$ positive cells (a marker for dendritic cells) due to their critical role in eliciting adaptive immune response which are mainly Langerhans cells and dermal dendritic cells (43, 47). Our analysis showed that 46.2 ± 8.16% of the OVA-expressing cells were DCs, confirming the successful transfection of DCs with the OVA plasmid (*SI Appendix*, Fig. S11*C*). While we have focused on $CD11c^+$ APCs, this emphasis does not rule out the possibility of using μEPO to transfect other cell types in the dermis and epidermis.

Such a low invasiveness ensures the least disturbance to cells' normal function and homeostasis, providing a good alternative for manufacturing therapeutic cells beyond the vaccination application demonstrated here. For example, in most of the current clinical practices involving engineered T cells, ex vivo cell manipulation remains a prerequisite, when the human donor-derived T cells are encapsulated in the 3D hydrogel, they can be μEPO-engineered to promote the production of tumor-targeting chimeric antibody receptor (CAR) T cells. If the μEPO application site is adapted from skin to specific T cell enriched tissues (e.g., lymph nodes), the minimally invasive procedures may be further developed to accommodate an in vivo T cell engineering approach that bypasses many uncertainties of in vitro cell manipulation and dramatically simplifies the therapeutic process involving CAR-T. Similar to the transdermal demonstration in this study, a brief dual-phase electrical stimulation would allow the release and intracellular delivery of therapeutic nucleic acids into relevant immune cells, such as T cells, to create CAR-T cells directly in the human body. It is reasonably expected that the convenience of such an in vivo cell engineering system would not only improve patients' compliance but also make it possible for repeated treatment if mRNAs are to be introduced for insertion-free gene editing (48, 49).

For studying cancer immunotherapy, OVA has been utilized as a model antigen to evaluate the efficacy of vaccine delivery, owing to its well-established antigenic nature and strong capacity to induce cellular immunity (via T cells) and humoral immunity (via B cells) (37). Our use of the OVA-DNAs and the melanoma cancer model was intended to provide a demonstrative application of the μEPO platform, which was developed as a general technology for transdermal delivery of nucleic acid materials into relevant cells for vaccination purposes. Specifically in this study, the μEPO device has been specifically explored for transdermal DNA vaccination in the B16-OVA melanoma mouse model. After the antigen-specific gene (i.e., OVA) was delivered to the immune cells by μEPO, we evaluated the tumor-specific immune response and antitumor efficacy. Notably, we also show that the electroporation plays an important role in the processes of APCs recruitment, antigen delivery, APCs activation, and cross-presentation, which effectively induces antigen-specific T cell response, CTLs response, and tumor inhibition, in virtue of the one-step transdermal gene delivery by using the μEPO platform.

Though not achieving tumor-free outcomes in mice that received OVA plasmid DNA vaccines, emerging evidence has suggested that the efficacy of cancer vaccines should also be judged by the impact on tumor growth kinetics, immune cell infiltration, and overall survival, especially in highly aggressive and poorly immunogenic tumor models like B16-OVA (50). Our demonstration with the μEPO platform provides valuable insights into the immunological responses induced by highly efficient delivery of DNA vaccine encoding the OVA antigen. In both prophylactic and therapeutic procedures, our technique achieved a remarkable tumor inhibition, prolonged survival, and enhanced T cell infiltration into the tumors, which provide a strong basis to support the efficacy of the nucleic acid-based therapeutics and associated transdermal delivery strategy. Moving forward, we believe that relevant cytokines or checkpoint inhibitors can be combined with the μEPO-DNA vaccination to further enhance its efficacy in combating tumor growth and improving overall cancer treatment based on immunotherapies.

In comparison with the currently existing immunotherapeutic practices (3, 5), the μEPO technique displays several distinct advantages. First, the μEPO-facilitated transdermal delivery of the OVA gene can effectively activate systemic immune responses to target tumors, not only superficial tumors but also nonepidermal ones, which is a clinically more legitimate alternative over intratumoral delivery of cancer vaccines. Second, the demonstrated in vivo electroporation can be readily extended to deliver a wide range of genetic cargos (protein, peptide, mRNA, toxoid, and reprogramming factors, etc.) for cancer immunotherapy, and the dose, timing, and treatment frequency can be easily optimized to improve the therapeutic outcome. While we only studied single OVA genes as a vaccine, plasmid DNAs encoding multiple neoantigens can be explored to elicit more robust and extensive antitumor-specific responses. Especially for highly malignant cancers (e.g., breast cancer and melanoma), neoantigens raised from tumors-specific mutations can be clinically used in personalized cancer immunotherapies (51). As a ready extension of this study, the μEPO platform can be designed to encapsulate and deliver DNA or RNA encoding other tumor-specific antigens beyond OVA, making it a versatile tool for improving cancer immunotherapy using nucleic acid materials. Proper antigen design would enable targeting not only epidermal but also nonepidermal tumors (3). For example, DNA encoding human prostatic acid phosphatase (PAP) is being developed as a vaccine to treat prostate cancer patients (52). Carcinoembryonic antigen (CEA) gene and HER2 gene are also clinically tested for fighting colorectal cancer or breast cancer, respectively, by adopting a DNA vaccine strategy (53). We believe that future studies to explore this versatility would provide

more comprehensive evidence to show μEPO's applicability in diverse cancer immunotherapy. The μEPO technique can extend such treatments with unprecedented precision, convenience, and efficiency via a self-administrative transdermal gene delivery process. A complex combination of antigen/adjuvants/cytokines can also be loaded in the μEPO devices for codelivery, which will certainly inspire safe and effective synergetic treatments. On a broader horizon beyond cancer immunotherapy, it is reasonably expected that the μEPO device can be further developed as a rapid and painless vaccination system for emerging infectious diseases, including COVID-19.

In sum, we develop a hydrogel electronic μEPO system to accommodate highly efficient, minimally invasive, transdermal gene delivery to subcutaneous cells. The transdermal injection and intracellular introduction of biologic molecules are performed by a one-step operation using a microarrayed in vivo electroporation, which is effectively operated in a nonviral and transfecting-reagent-free format. Oriented toward cancer immunotherapy, the μEPO system can be used for transdermal delivery of antigen-specific genes to subcutaneous cells to activate systemic immune response for cancer prevention and therapy. It is believed that the μEPO system would be of great translational value for different therapeutic purposes that involve in vivo delivery of different biological therapeutics.

Methods

Cell Line and Animal. HEK293T cells and B16 melanoma cell line transfected with ovalbumin (B16-OVA) cells were cultured in Dulbecco's modified Eagle's medium (DMEM) with 10% fetal bovine serum (FBS) and 1% penicillin/streptomycin (PS) at 37 °C in 5% CO_2.

All animal procedures were approved by the Animal Ethical Committee of City University of Hong Kong (CityU) and Department of Health of Hong Kong. Female C57BL/6 mice (6 to 8 wk) were acquired from the Laboratory Animal Research Unit (LARU) of CityU and were maintained following standard guidelines.

Fabrication of the μEPO Device. The microneedle electrodes used in this study were fabricated using polydimethylsiloxane (PDMS) micromolds purchased from Micropoint Technologies Pte Ltd (Singapore). The needle was arranged in a 10 × 10 array with an 800 μm center-to-center space. Each needle cavity was pyramid in shape with a base diameter of 400 μm, a height of 1,000 μm. 15 *wt*% of PVA and 0.3 *wt*% PEDOT:PSS was dissolved in DEPC water under 95 °C for 3 h to get a homogeneous hydrogel solution. Then, the macromolecules were added into the hydrogel solution, followed by the addition into the plasma-treated PDMS cavity, which would be regarded as the therapeutic layer. After drying at room temperature in a fume hood (about 3 h), the hydrogel solution was added into PDMS mold to fill up the base, forming the back layer. The PDMS mold was placed into a fume hood for 24 h to get a completely dried patch. After that, the μEPO device was carefully detached from the mold. To enable better connection with the pulse generator, the manicured microneedle layer was fixed on the conductive tape with manufactured trimmed. Finally, the obtained device was mounted on medical tape for further protection and portable use.

In Vivo Gene Expression. The day before the insertion, the mice were shaved, and the depilator cream was applied for achieving hair removal. The mice were placed under anesthesia using isoflurane (5% for induction and 3% for maintenance), and the μEPO device was pressed into the skin. A negative voltage (−1 V) was applied to the μEPO device for 10 min to trigger DNA release. Pulsed electrical stimulation (10 pulses, 90 V in amplitude, 50 ms/pulse) was then applied to facilitate the in vivo electroporation into cells. To assess eGFP expression, the skin samples were collected, embedded in OCT, sectioned, and mounted to charged microscopy slides. Subsequently, the OCT-embedded skin sections were treated with 4% paraformaldehyde at 4 °C for fixation, followed by staining with DAPI. To assess OVA expression, the skin samples were harvested, embedded in OCT, sectioned, and mounted to charged microscopy slides. We leverage specific antibodies to detect and visualize the colocalization of OVA protein in $CD11c^+$ APCs in treated subcutaneous regions, given their pivotal role in eliciting adaptive immune response. We used anti-ovalbumin antibody (Abcam, ab181688) to target OVA antigen and anti-CD11c monoclonal antibody (N418, eBiosclence) to identify $CD11c^+$ DCs. The OCT-embedded skin sections were treated with 4% paraformaldehyde at 4 °C, permeabilized, and blocked with 3% BSA in 0.25% Triton X-100 (v:v% in PBS) at room temperature. Cells were stained overnight using CD11c monoclonal antibody and anti-Ovalbumin antibody, subsequently incubated with fluorescence-tagged secondary antibodies at room temperature for 2 h to visualize OVA expression within $CD11c^+$ cells under fluorescence microscopy. The fluorescence images were captured by a laser scanning confocal microscope (Leica SP8).

Vaccination. All experiments involving animals were approved by the Animal Ethics Committee of the City University of Hong Kong and conducted following the health guide for the care and use of laboratory animals. Female C57BL/6 mice (6 to 8 wk old) were randomly divided into different groups: i) immunized with OVA plasmid-loaded μEPO device with electroporation (labeled as OVA-ELE); ii) immunized with OVA plasmid-loaded μEPO device without electroporation (labeled as OVA); iii) immunized with μEPO device with electroporation but without OVA plasmid loading (labeled as ELE); iv) intramuscular injection of OVA plasmid (IM); v) intramuscular injection of lipofectamine plus OVA plasmid formulation (Lipo); vi) intramuscular injection of OVA plasmid plus bulk electroporation (IM-bEP); vii) subdermal injection of OVA plasmid plus bulk electroporation (SD-bEP) and viii) untreated group. The areas to be treated were shaved; depilatory cream was applied 1 d before immunization. For bulk in vivo electroporation group, the mice were briefly anesthetized and subjected to electroporation using the BTX electroporator (BTX, ECM 830, 10 × 20 ms/pulses, 200 V/cm). The electrodes were applied to the targeted skin area immediately after DNA injection. For μEPO treated groups, the devices were pressed against the animal's back skin, and a negative voltage (1 V) was applied for 10 min, then followed by pulsed electrical stimulation (10 pulses, 90 V, 50 ms/pulse). In this process, a platinum electrode was juxtaposed to the μEPO device by using a magnet. Each animal received multiple μEPO treatment, a second or third dosing was applied at 1-wk intervals.

In Vivo Cancer Prophylactic and Therapeutic Studies. To assess the prophylactic efficacy of the μEPO device, C57BL/6 mice were vaccinated with either the OVA-ELE (10 μg DNA/patch), OVA (10 μg DNA/patch, no electrical stimulation), ELE (no DNA/patch, with electrical stimulation), IM (10 μg OVA DNA in 100 μL PBS), or left untreated. The mice were vaccinated three times at 1-wk intervals. Seven days after the final vaccination, the vaccinated mice were inoculated subcutaneously with 3×10^5 B16-OVA melanoma cells into the back of the mice.

To assess the in vivo therapeutic efficacy of the μEPO device, C57BL/6 mice were inoculated subcutaneously with 3×10^5 B16-OVA melanoma cells into the back of mice on day 0. Tumors were allowed to grow for 5 d, and these tumor-bearing mice were randomly divided into five groups. On days 5, 12, and 19, the mice were vaccinated with different conditions, as described in the above text.

Tumors were monitored every 3 d using calipers in three dimensions. Tumor volumes were calculated using the formula $V = 0.5 \times L \times S^2$, where L and S are the larger and smaller diameters, respectively. Mice were sacrificed when the tumor volumes reached 2,000 mm^3.

Statistical Analysis. All the experimental data in this study were subjected to statistical analysis and were expressed as mean ± SEM. The statistical significance ($*P < 0.05$, $***P < 0.001$) was determined using Student's *t* test, unless otherwise specified in the text.

Data, Materials, and Software Availability. All study data are included in the article and/or *SI Appendix*.

ACKNOWLEDGMENTS. This work was supported by National Natural Science Foundation of China (U20A20194), by Science Technology and Innovation Commission of Shenzhen Municipality (SGDX20201103093005O2), and by General Research Fund (11215920, 11218522, 11218523) from the Research Grants Council of Hong Kong SAR. Support from Innovation and Technology Commission of Hong Kong through the Centre for Cerebro-Cardiovascular Health Engineering and funds from City University of Hong Kong (7030011, 7005084, 7005206, 7005642, 7020003, 7020077, 9680323, 9240060) are also acknowledged.

Author affiliations: [a]Department of Biomedical Engineering, City University of Hong Kong, Kowloon, Hong Kong Special Administrative Region 999077, China; [b]Department of Materials Science and Engineering, City University of Hong Kong, Kowloon, Hong Kong Special Administrative Region 999077, China; [c]Department of Chemistry, City University of Hong Kong, Kowloon, Hong Kong Special Administrative Region 999077, China; [d]Department of Chemical and Biological Engineering, The Hong Kong University of Science and Technology, Kowloon, Hong Kong Special Administrative Region 999077, China; [e]Department of Mechanical and Aerospace Engineering, The Hong Kong University of Science and Technology, Hong Kong Special Administrative Region 999077, China; [f]Center of Super-Diamond and Advanced Films, City University of Hong Kong, Kowloon, Hong Kong Special Administrative Region 999077, China; [g]Hong Kong Centre for Cerebro-Cardiovascular Health Engineering, Hong Kong Special Administrative Region 999077, China; and [h]Shenzhen Research Institute, City University of Hong Kong, Shenzhen 518000, China

Author contributions: Y.W., J.Q., and P.S. designed research; Y.W., J.Q., C.X., and Z.Y. performed research; B.C., M.W., Z. Liu, Z. Liang, F.W., T.Z., G.Z., and Y.B.K. contributed new reagents/analytic tools; Y.W., J.Q., K.X., and P.S. analyzed data; and Y.W., J.Q., and P.S. wrote the paper.

1. A. D. Waldman, J. M. Fritz, M. J. Lenardo, A guide to cancer immunotherapy: From T cell basic science to clinical practice. *Nat. Rev. Immunol.* **20**, 651–668 (2020).
2. L. Scheetz *et al.*, Engineering patient-specific cancer immunotherapies. *Nat. Biomed. Eng.* **3**, 768–782 (2019).
3. Z. Hu, P. A. Ott, C. J. Wu, Towards personalized, tumour-specific, therapeutic vaccines for cancer. *Nat. Rev. Immunol.* **18**, 168–182 (2018).
4. J. R. Gregg, T. C. Thompson, Considering the potential for gene-based therapy in prostate cancer. *Nat. Rev. Urol.* **18**, 170–184 (2021).
5. R. S. Riley, C. H. June, R. Langer, M. J. Mitchell, Delivery technologies for cancer immunotherapy. *Nat. Rev. Drug Discov.* **18**, 175–196 (2019).
6. G. Zhu, F. Zhang, Q. Ni, G. Niu, X. Chen, Efficient nanovaccine delivery in cancer immunotherapy. *ACS Nano* **11**, 2387–2392 (2017).
7. T. L. Nguyen, Y. Yin, Y. Choi, J. H. Jeong, J. Kim, Enhanced cancer DNA vaccine via direct transfection to host dendritic cells recruited in injectable scaffolds. *ACS Nano* **14**, 11623–11636 (2020).
8. D. Eusebio *et al.*, Methods to improve the immunogenicity of plasmid DNA vaccines. *Drug Discov. Today* **26**, 2575–2592 (2021).
9. M. Shafaati *et al.*, A brief review on DNA vaccines in the era of COVID-19. *Future Virol.* **17**, 49–66 (2021).
10. R. Kumar *et al.*, Polymeric delivery of therapeutic nucleic acids. *Chem. Rev.* **121**, 11527–11652 (2021).
11. J. Rice, C. H. Ottensmeier, F. K. Stevenson, DNA vaccines: Precision tools for activating effective immunity against cancer. *Nat. Rev. Cancer* **8**, 108–120 (2008).
12. Y. Wang *et al.*, Poking cells for efficient vector-free intracellular delivery. *Nat. Commun.* **5**, 4466 (2014).
13. X. Hou, T. Zaks, R. Langer, Y. Dong, Lipid nanoparticles for mRNA delivery. *Nat. Rev. Mater.* **6**, 1078–1094 (2021).
14. J. Szebeni *et al.*, Applying lessons learned from nanomedicines to understand rare hypersensitivity reactions to mRNA-based SARS-CoV-2 vaccines. *Nat. Nanotechnol.* **17**, 337–346 (2022).
15. D. Morshedi Rad *et al.*, A comprehensive review on intracellular delivery. *Adv. Mater.* **33**, e2005363 (2021).
16. A. Brave, S. Nystrom, A. K. Roos, S. E. Applequist, Plasmid DNA vaccination using skin electroporation promotes poly-functional CD4 T-cell responses. *Immunol. Cell Biol.* **89**, 492–496 (2011).
17. P. G. Popova, S. P. Chen, S. Liao, M. Sadarangani, A. K. Blakney, Clinical perspective on topical vaccination strategies. *Adv. Drug Deliv. Rev.* **208**, 115292 (2024).
18. P. C. DeMuth *et al.*, Polymer multilayer tattooing for enhanced DNA vaccination. *Nat. Mater.* **12**, 367–376 (2013).
19. J. Fang *et al.*, Engineering biomaterials with micro/nanotechnologies for cell reprogramming. *ACS Nano* **14**, 1296–1318 (2020).
20. K. T. M. Tran *et al.*, Transdermal microneedles for the programmable burst release of multiple vaccine payloads. *Nat. Biomed. Eng.* **5**, 998–1007 (2021).
21. E. Korkmaz *et al.*, Microarray patches enable the development of skin-targeted vaccines against COVID-19. *Adv. Drug Deliv. Rev.* **171**, 164–186 (2021).
22. L. Engelke, G. Winter, S. Hook, J. Engert, Recent insights into cutaneous immunization: How to vaccinate via the skin. *Vaccine* **33**, 4663–4674 (2015).
23. Z. Zhao, A. Ukidve, A. Dasgupta, S. Mitragotri, Transdermal immunomodulation: Principles, advances and perspectives. *Adv. Drug Deliv. Rev.* **127**, 3–19 (2018).
24. D. Li *et al.*, Progress and perspective of microneedle system for anti-cancer drug delivery. *Biomaterials* **264**, 120410 (2021).
25. D. Xia *et al.*, An ultra-low-cost electroporator with microneedle electrodes (ePatch) for SARS-CoV-2 vaccination. *Proc. Natl. Acad. Sci. U.S.A.* **118**, e2110817118 (2021).
26. M. A. Kutzler, D. B. Weiner, DNA vaccines: Ready for prime time? *Nat. Rev. Genet.* **9**, 776–788 (2008).
27. M. Zheng, T. Sheng, J. Yu, Z. Gu, C. Xu, Microneedle biomedical devices. *Nat. Rev. Bioeng.* **2**, 324–342 (2023).
28. T. R. F. Smith *et al.*, Immunogenicity of a DNA vaccine candidate for COVID-19. *Nat. Commun.* **11**, 2601 (2020).
29. Z. Chen *et al.*, Bioorthogonal catalytic patch. *Nat. Nanotechnol.* **16**, 933–941 (2021).
30. K. Xie *et al.*, Organic electrochemical transistor arrays for real-time mapping of evoked neurotransmitter release in vivo. *Elife* **9**, e50345 (2020).
31. D. Gallego-Perez *et al.*, Topical tissue nano-transfection mediates non-viral stroma reprogramming and rescue. *Nat. Nanotechnol.* **12**, 974–979 (2017).
32. Z. Wang *et al.*, Microneedle patch for the ultrasensitive quantification of protein biomarkers in interstitial fluid. *Nat. Biomed. Eng.* **5**, 64–76 (2021).
33. S. Kusama *et al.*, Transdermal electroosmotic flow generated by a porous microneedle array patch. *Nat. Commun.* **12**, 658 (2021).
34. G. A. Roth *et al.*, Designing spatial and temporal control of vaccine responses. *Nat. Rev. Mater.* **7**, 174–195 (2022).
35. J. Zhu, Y.-J. Ren, Tuning the plasmon shift and local electric field distribution of gold nanodumbbell: The effect of surface curvature transition from positive to negative. *Appl. Surf. Sci.* **285**, 649–656 (2013).
36. A. Gothelf, J. Gehl, Gene electrotransfer to skin; review of existing literature and clinical perspectives. *Curr. Gene Ther.* **10**, 287–299 (2010).
37. J. Xu *et al.*, A general strategy towards personalized nanovaccines based on fluoropolymers for post-surgical cancer immunotherapy. *Nat. Nanotechnol.* **15**, 1043–1052 (2020).
38. M. Super *et al.*, Biomaterial vaccines capturing pathogen-associated molecular patterns protect against bacterial infections and septic shock. *Nat. Biomed. Eng.* **6**, 8–18 (2022).
39. L. M. Kranz *et al.*, Systemic RNA delivery to dendritic cells exploits antiviral defence for cancer immunotherapy. *Nature* **534**, 396–401 (2016).
40. S. Liu *et al.*, A DNA nanodevice-based vaccine for cancer immunotherapy. *Nat. Mater.* **20**, 421–430 (2021).
41. J. Koerner *et al.*, PLGA-particle vaccine carrying TLR3/RIG-I ligand Riboxxim synergizes with immune checkpoint blockade for effective anti-cancer immunotherapy. *Nat. Commun.* **12**, 2935 (2021).
42. M. Staples, Microchips and controlled-release drug reservoirs. *Wiley Interdiscip. Rev. Nanomed. Nanobiotechnol.* **2**, 400–417 (2010).
43. Y. C. Kim, J. H. Park, M. R. Prausnitz, Microneedles for drug and vaccine delivery. *Adv. Drug Deliv. Rev.* **64**, 1547–1568 (2012).
44. B. Z. Chen, L. Q. Zhang, Y. Y. Xia, X. P. Zhang, X. D. Guo, A basal-bolus insulin regimen integrated microneedle patch for intraday postprandial glucose control. *Sci. Adv.* **6**, eaba7260 (2020).
45. W. Li *et al.*, Rapidly separable microneedle patch for the sustained release of a contraceptive. *Nat. Biomed. Eng.* **3**, 220–229 (2019).
46. J. Zhang *et al.*, Microneedle-enabled therapeutics delivery and biosensing in clinical trials. *J. Controll. Release* **360**, 687–704 (2023).
47. J. Wu, H. Wu, J. An, C. M. Ballantyne, J. G. Cyster, Critical role of integrin CD11c in splenic dendritic cell capture of missing-self CD47 cells to induce adaptive immunity. *Proc. Natl. Acad. Sci. U.S.A.* **115**, 6786–6791 (2018).
48. C. H. June, R. S. O'Connor, O. U. Kawalekar, S. Ghassemi, M. C. Milone, CAR T cell immunotherapy for human cancer. *Science* **359**, 1361–1365 (2018).
49. J. A. Doudna, The promise and challenge of therapeutic genome editing. *Nature* **578**, 229–236 (2020).
50. P. Zhou *et al.*, In vivo discovery of immunotherapy targets in the tumour microenvironment. *Nature* **506**, 52–57 (2014).
51. E. Blass, P. A. Ott, Advances in the development of personalized neoantigen-based therapeutic cancer vaccines. *Nat. Rev. Clin. Oncol.* **18**, 215–229 (2021).
52. D. G. McNeel *et al.*, Safety and immunological efficacy of a DNA vaccine encoding prostatic acid phosphatase in patients with stage D0 prostate cancer. *J. Clin. Oncol.* **27**, 4047–4054 (2009).
53. B. Yang, J. Jeang, A. Yang, T. C. Wu, C. F. Hung, DNA vaccine for cancer immunotherapy. *Hum. Vaccines Immunother.* **10**, 3153–3164 (2014).